Desalination and Water Treatment
www.deswater.com

doi: 10.5004/dwt.2021.26493

209 (2021) 280–288
January

Fixed bed column adsorption of vanadium from water using amino-functional polymeric adsorbent

Serdar Aydın[a,*], Hamda Mowlid Nur[a], Abdoulaye Mamadou Traore[a], Eren Yıldırım[b], Serkan Emik[b]

[a]*Department of Environmental Engineering, Faculty of Engineering, Istanbul University-Cerrahpaşa, Istanbul, Turkey, Tel. +90 212 473 70 70; Fax: +90 212 473 71 80; emails: saydin@istanbul.edu.tr (S. Aydın), masniitah@gmail.com (H.M. Nur), amtraore93@gmail.com (A.M. Traore)*
[b]*Department of Chemical Engineering, Istanbul University-Cerrahpaşa, Istanbul, Turkey, emails: erenyildirim@istanbul.edu.tr (E. Yıldırım), s.emik@istanbul.edu.tr (S. Emik)*

Received 1 June 2020; Accepted 22 August 2020

ABSTRACT

Vanadium is listed on candidate contaminant list (CCL), and regulatory guidelines exist for vanadium in some countries. Previous studies have examined vanadium adsorption in batch studies, but limited knowledge is available for column adsorption of vanadium. As communities are moving towards potable water reuse, column adsorption treatment is and will play a vital role in water reuse. This paper assesses vanadium removal by amino poly glycidyl methacrylate (amino-pGMA) in fixed-bed column adsorption. The effects of influent vanadium concentration (50–100 mg/L), feed flow rate (7.5–12.5 mL/min), and amino-pGMA bed height (2–4 cm) on the breakthrough characteristics of the adsorption system were determined. The highest bed capacity of 75.5 mg/g was obtained using 75 mg/L influent vanadium concentration, 2 cm bed height, and 7.5 mL/min flow rate. The adsorption data were fitted to three well-established fixed-bed adsorption models, namely: Thomas, Yoon–Nelson, and bed depth service time (BDST) models. The results were compared to the experimentally attained data, and they elicited an excellent fit for all the models ($R^2 \geq 0.90$) at different conditions. The findings suggested that amino-pGMA in fixed-bed column adsorption presents great potential in the removal of vanadium from water. The amino group on the adsorbent played a cardinal role in the adsorption of vanadium.

Keywords: Fixed bed column; Amino functionalized polymers; Vanadium removal; Adsorption

1. Introduction

Vanadium is a rare earth element that has been used extensively as an alloy in steel, jet, and high-speed aircraft manufacturing. In addition, it is used as a superconducting magnet as a catalyst in the production of sulphuric acid, and vanadium been reported to be an efficient energy storage material [1–3]. With these developments, vanadium concentrations in water are on the rise. Also, vanadium is widely distributed in the earth's crust and has been recognized as a potentially dangerous contaminant in the same class as mercury, lead, and arsenic [4]. Elevated concentrations have been linked to depression, a condition that can cause severe shifts in the mood, and excess mucus production. Vanadium can also be easily associated with common anions found in water such as sulfate and chlorides, and when related to such anions, the resulting compounds can lead to a series of health hazards such as dermatitis, flushing, hypotension,

* Corresponding author.

abdominal pain, and as well as environmental risks such as eutrophication [5,6]. It is, therefore, essential to treat vanadium salt polluted wastewater before it is dumped into any water body.

Traditional methods of treating polluted water include physical, chemical, and biological techniques [7–10]. However, physical–chemical methods offer higher efficacy compared to biological processes. Ion-exchange and adsorption techniques have become the most reliable choice when treating wastewater that contains metal ions [11,12]; the latter offers a competitive advantage during the implementation phase [13]. There are two main adsorption approaches, batch, and continuous-column adsorption. The batch adsorption process is easy to operate. However, the batch process requires sedimentation and/or filtration chamber if continuous wastewater treatment is to be implemented; this escalates the cost of the batch process. The continuous adsorption in a fixed-bed column is often desired from an industrial point of view. A continuous packed bed does not run under equilibrium conditions like the batch process. In addition, *in situ* regeneration of adsorbent within the column reduces down-time and offers cost-benefit. To design and operate a fixed-bed adsorption process successfully, breakthrough curves under specified operating conditions must be predictable. The shape of the curve is influenced by individual transport process in the column and the adsorbent. Breakthrough determines bed height and the operating life span of the bed and regeneration time.

Numerous commercially produced adsorbents exist; however, the choice of an adsorbent depends on its availability, cost, and efficiency. Industrial adsorbents are classified based on oxygen-containing, carbon-based, and polymer-based adsorbent [14]. When adequately prepared, polymer-based adsorbents offer a competitive removal of metal ions under extreme environmental conditions. The use of polymers as an adsorbent is of great interest because of their efficiency and affordability [15]. Poly-glycidyl methacrylate (pGMA) is a polymer matrix that has resistance to acids and alkali, and also has a strong porous structure [16]. The interpenetrating polymer network that makes pGMA can serve as a great polymeric adsorbent. Modification is necessary to enhance the polymer related adsorbents. Adsorbents modified with amine related groups have proven to be superior adsorbents during anion and/or anion removal from wastewater [7,15]. In this study, vanadium removal studies were carried out on laboratory-scale using a fixed-bed column with an amino-functionalized polymeric adsorbent resin. The effect of bed height, feed flow rate, and initial concentration on the adsorption process were examined. The breakthrough curves were analyzed using Thomas, Yoon–Nelson, and bed-depth service time model equations [17–19].

2. Materials and methods

2.1. Chemicals

Glycidyl methacrylate (GMA), ethylene glycol dimetahacrylate (EGDM), benzoyl peroxide (BPO), mercury(II) nitrate ($Hg(NO_3)_2$), gallic acid ($H_6C_7O_5$), and ammonium metavanadate (NH_4VO_3) were obtained in their pure or analytical grade and were purchased from Merck Chemicals (Germany). Where necessary, the pH was adjusted with dilute HCl or NaOH solutions, and in all the experiments, distilled water was used.

2.2. Preparation and characterization of the adsorbent

The synthesis procedure of the amino-functional adsorbent involved two main steps, as illustrated in Fig. 1. The first step is the bulk polymerization of GMA, and the crosslinker EGDM at a mole ratio of 20:1. Briefly, free radical crosslinking polymerization of GMA was carried out at 80°C, and 3 h using initiator BPO (1% mol of the total monomer amount) [16]. After the reaction period, the crosslinked polymer was disintegrated in cold methanol and dried in a vacuum oven at 30°C. In the second step, the amination process of crosslinked pGMA was done by the epoxy ring-opening process. To get amino-functionalized pGMA resin, 1.0 g of pGMA, and 10.0 g dimethylformamide (DMF) were put into a reactor, and the reaction solution degassed for 15 min with nitrogen. 4.0 g of EDA was put into the reaction mixture, and the closed air-tight test-tube was submerged in a stable water bath at 80°C. Twelve hours later, this mixture product was filtered and washed independently with ethanol three times, then by ethanol-water (50:50, w:w) solution, and finally with water. The product (amino-pGMA) was dried-out at 30°C in an oven, milled and sieved through a size of 350–500 mesh. Fig. 1 elicits the formation of amino-pGMA in the reactor. The amine value (AV) of the adsorbent was determined as reported in the literature [16] and found to be 330 ± 5 mg KOH/g adsorbent (~6 mmol/g). An Agilent Cary 630 (USA) model Fourier transform infrared spectroscopy (FTIR) was used to study the chemical characterization of the adsorbent before and after adsorption. A thermo-gravimetric analyzer (TGA) (model: LINSEIS STA PT1750) was used to analyze the thermal behavior of the products.

2.3. Dynamic adsorption studies and procedure

Continuous flow adsorption experiments were conducted in a glass tube with an internal diameter of 1.1 cm. A known amount of amino-functionalized polymers was sealed tight in a glass column with glass wool to yield the desired bed height of 2, 3, and 4 cm, equivalent to 2, 3, and 4 g of amino-pGMA, respectively. The column was then filled with glass beads to provide a uniform flow of the solution through the column. Vanadium solution of known concentrations (50, 75, and 100 mg/L) at pH 4.5 was pumped upward through the column at the desired flow rate (7.5, 10, and 12.5 mL/min) controlled by a peristaltic pump shown in Fig. 2. Vanadium solution at the outlet of the column was collected at regular time intervals (10 min), and the effluent concentration was measured using the gallic acid method as described by [1]. The experiments were carried out at 20°C ± 2°C. Breakthrough curves show the loading behavior of the target contaminant to be removed from the solution in a fixed bed. It is commonly described in terms of adsorbed contaminant concentration (C_{ad}) or as the ratio of effluent contaminant concentration to influent concentration (C_t/C_0) as a function of time or volume of effluent for a given bed height [20]. The dynamic adsorption capacity of amino-pGMA was determined using Eqs. (1)–(3).

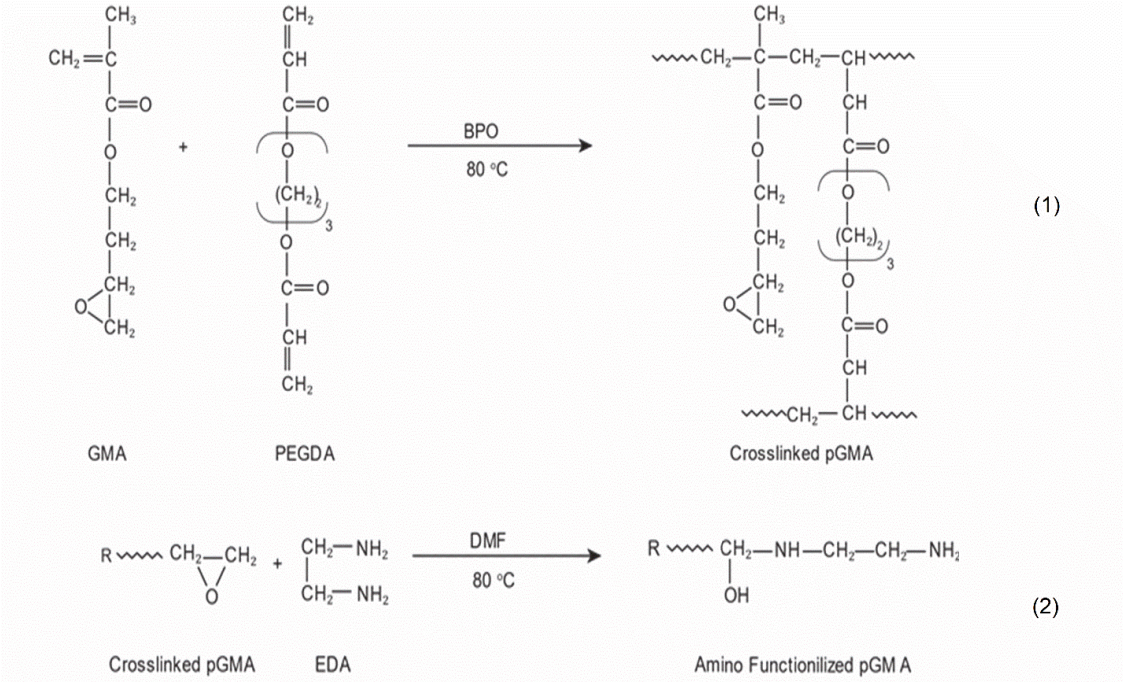

Fig. 1. Schematic illustration of the synthesis reaction [16].

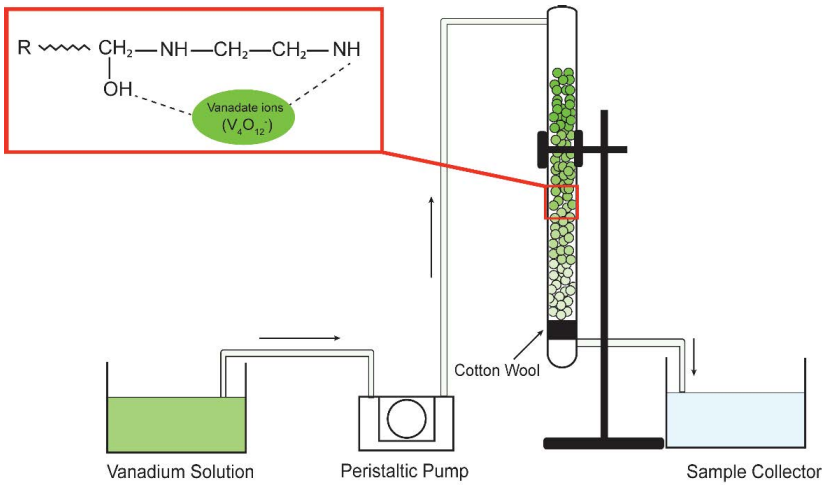

Fig. 2. Fixed bed column design, internal diameter: 1.1 cm, column height: 2–4 cm, flowrate: 7.5–12.5 mL/min, and initial concentration: 50–100 mg/L.

$$Q_{\text{total}} = \frac{QA}{1{,}000} = \frac{Q}{1{,}000}\int_{t=0}^{t=e} C_{\text{ad}}\,dt \quad (1)$$

$$V_{\text{eff}} = Q \cdot t_e \quad (2)$$

$$q_e = \frac{Q_{\text{total}}}{X} \quad (3)$$

where q_e is the adsorption capacity (mg/g); Q_{total} is the total amount of contaminant sorbed (mg); X is the mass of sorbent (g); V_{eff} is the volume of the effluent; A is the area; t_e is the column exhaustion time (min); Q is the volumetric flow-rate (mL min^{-1}); C_{ad} is the adsorbed concentration (mg/L).

2.4. Mathematical models used in the study

In this study, three mathematical models were used, that is, Thomas, Yoon–Nelson, and bed-depth service time model [17–19]. Table 1 illustrates the models with following equations used to attain theoretical values for each condition.

3. Results and discussion

3.1. Characterization studies

The FTIR spectrum of the synthesized product is shown in Fig. 3. Fig. 3a shows pGMA spectrum with two characteristic peaks at 1,725 and 1,255 cm^{-1}, which correspond to C=O stretching and C–O–C stretching vibration of

Table 1
Model equations used to calculate the theoretical values

Model	Equation	Plot	Model Parameter
Thomas	$\frac{C_t}{C_0}=\frac{1}{1+\exp\left(\frac{K_{TH}q_0x}{Q-C_0V_{eff}t}\right)}$	$\ln((C_0/C_t)-1)$ vs. t	K_{TH} q_0
Bed depth service time	$t=\frac{N_0}{C_0F}Z-\frac{1}{K_{BDST}C_0}\ln\left(\frac{C_0}{C_t}-1\right)$	Z vs. t	N_0 K_{BDST}
Yoon–Nelson	$\frac{C_t}{C_0}=\exp\left(K_{YN}t-\tau K_{YN}\right)$	$\ln\left(\frac{C_1}{C_0-C_t}\right)$ vs. t	K_{YN} T

C_0: initial concentration (mg/L); C_t: concentration at time t (mg/L); Q: volumetric flow rate (mL min^{-1}); K_{TH}: Thomas rate constant (mL min^{-1} mg^{-1}); q_0: uptake capacity (mg/g); x: the mass of adsorbent (g); K_{YN}: Yoon–Nelson rate constant (L min^{-1}); and τ: time required for 50% adsorbate breakthrough (min); K_{BDST}: bed depth service time rate constant (L/mg/h); N_0: bed capacity; T: time (min); F: linear flowrate (cm/h); Z: bed height (cm).

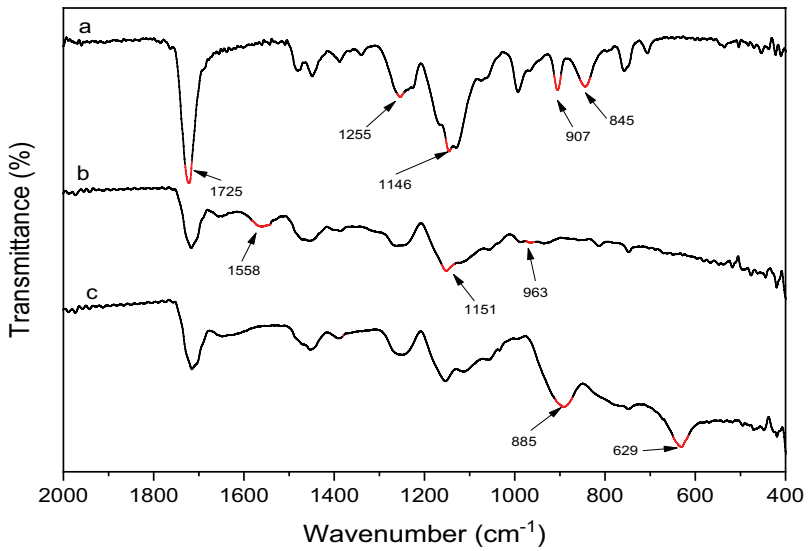

Fig. 3. FTIR spectra of (a) crosslinked pGMA, (b) amino-pGMA, and (c) amino-pGMA resin after the adsorption process.

ester groups, respectively. Besides, three weak bands at 1,255; 907; and 845 cm^{-1} correspond to the asymmetric stretching vibration of epoxide groups. After the amination reaction, Fig. 3b, the characteristic peak at 907 cm^{-1} for the epoxy group disappeared and depending on the incorporation of –NH_2 groups into the structure, new peaks at 1,558; 1,151; and 963 cm^{-1} was observed. These peaks correspond to N–H bending, C–N stretching, and N–H wag vibrations, respectively [16]. After the adsorption process, Fig. 3c, the spectrum of vanadium adsorbed resin showed new peaks, band shift, and intensity changes due to the adsorption. The formation of weak bands at 885 and 629 cm^{-1} also confirms the vanadium adsorption [1].

Fig. 4a elicits the thermal behavior of both pGMA and amino-pGMA; the presence of amino groups increases the thermal resistance pGMA [16]. Thermal oxidative degradation behaviors of pGMA and amino-pGMA are quite different from each other due to the chemical structure change after the amination process. A detailed analysis of the DTG curves (Fig. 4b) depicts two sharp peaks at 245°C, and 315°C; these peaks are attributed to the degradation of the epoxy groups and ester bonds, respectively. These two peaks became clearly undetectable due to the opening of the epoxy ring after the amination reaction. Since the presence of amino groups in the modified product will increase the adsorption of water, the peak of 140°C in the DTG curve is attributed to vaporization moisture.

3.2. Effect of influent vanadium concentration

The behavior of a fixed-bed column is best described with the concept of the breakthrough curve. Breakthrough appearance, time, and the shape of the breakthrough curve are the most significant traits for determining the

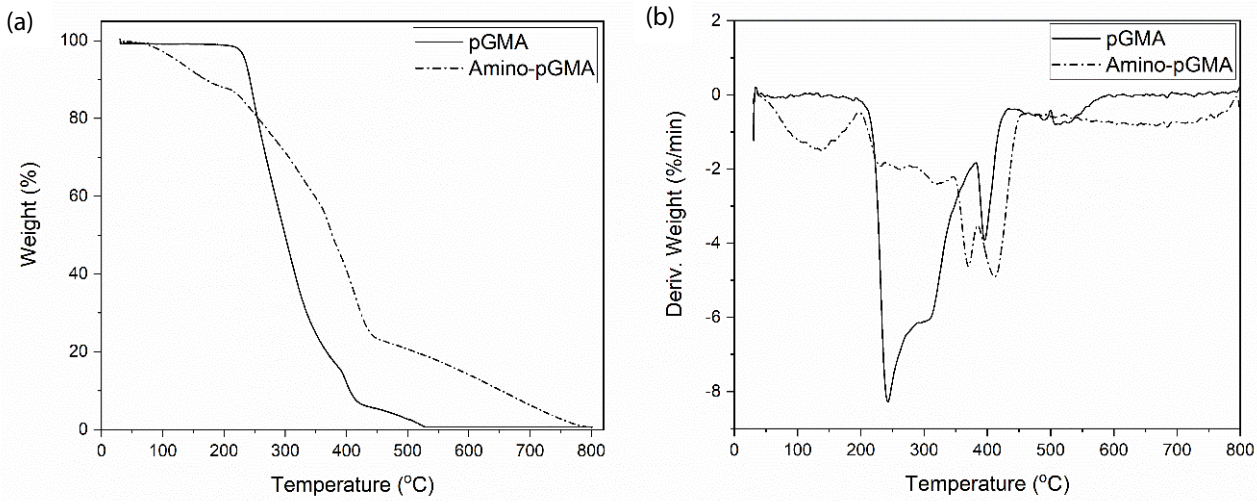

Fig. 4. (a) TGA and (b) difference thermogravimetry (DTG) analysis of pGMA and amino-pGMA. Conditions: 20 mg dried sample, 10°C/min heating rate, and dry air at 6 L/h flow rate.

operation and dynamic response of an adsorption column [21]. In addition, the most important parameters for a breakthrough curve study are the bed height, flow rate, and initial influent concentration. Thus, in the following sections, the effects of these parameters on the shape of the breakthrough curve and column performance were investigated. The effect of influent vanadium concentration (C_0) on the removal performance of the fixed-bed column containing amino-pGMA was examined at vanadium concentration of C_0 = 100, 75, and 50 mg/L. The experiments were carried out at a flow rate of 10 mL/min and a column bed height of 3 cm. As elicited in Fig. 5, within 60 min, the value of C_t/C_0 reached 0.80, 0.50, and 0.15 when influent concentration was 100, 75, and 50 mg/L, respectively. It is illustrated that the breakthrough time significantly decreased with increasing influent vanadium concentration.

At lower influent vanadium concentrations, breakthrough curves were dispersed, and the breakthrough occurred slower compared to high concentration. Higher concentration accelerates the diffusion and mass transfer coefficient [13]. Similarly, at lower influent concentration, the column bed exhaustion time is high, owing to the lower concentration gradient. These results demonstrate that the change of concentration gradient affects the saturation rate and breakthrough time; in other words, the diffusion process is concentration-dependent. As the influent concentration increases, the vanadium loading rate increases, so does the driving force increase for mass transfer, which decreases the adsorption zone length. The adsorption capacity was expected to increase with increasing the influent concentration because a high concentration difference provides a high driving force for the adsorption process. However, in this study, the highest bed capacity of 50.2 mg/g was obtained using 50 mg/L influent vanadium concentration, 3 cm bed height, and 10 mL/min flow rate. The uptake capacity (q_e) of the fixed-bed column decreased on increasing the influent concentration. Thus, the driving force for the adsorption is due to the concentration difference that exists between the amino-pGMA solid and liquid phase (adsorbent and adsorbate) [22]. Table 2 summarizes the dynamic adsorption parameters.

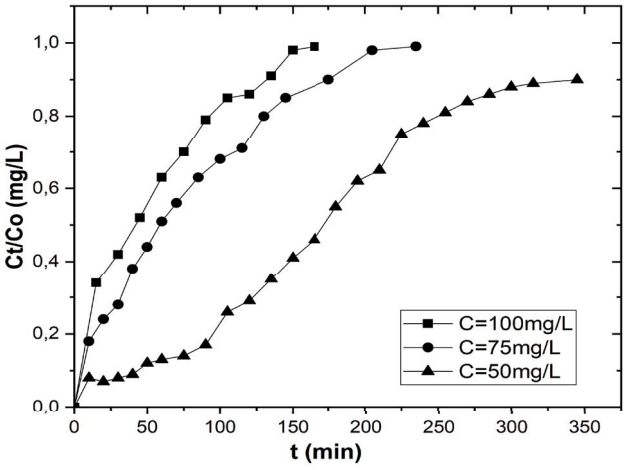

Fig. 5. Breakthrough curves for vanadium adsorption on prepared amino-pGMA at different influent concentrations (bed height = 3 cm, flow rate = 10 mL/min, pH = 4.5, and temperature = 22°C ± 1°C).

3.3. Effect of flow rate

The effect of flowrate, Q on dynamic adsorption of vanadium was investigated at Q = 7.5, 10, and 12.5 mL/min) while keeping constant bed height (3.0 cm) and influent vanadium concentration (75 mg/L). The breakthrough curves are represented in Fig. A1; it took less time to exhaust the column at a higher flow rate. The variation in the slope of the breakthrough and adsorption capacity curve can be explained on the basis of mass transfer fundamentals. As the flow rate increases, the residence time of the vanadium solution in the column bed decrease, inhibiting the diffusion of the vanadium toward stationary phase and pores

Table 2
Parameters influencing the dynamic adsorption of vanadium on amino-pGMA

Conditions	Variable	V_{eff} (mL)	t_e (min)	q_e (mg/g)
C_0 (mg/L) at Q = 10 mL/min	100.0	1,650.0	165.0	31.863
and Z = 3 cm	75.0	2,350.0	235.0	31.925
	50.0	3,450.0	345.0	50.188
Q (mL/min) at C_0 = 75 mg/L,	7.5.0	2,737.0	365.0	75.502
Z = 3 cm	10.0	2,350.0	235.0	31.925
	12.5	1,375.0	110.0	29.613
Bed height, Z (cm) at	2.0	2,600.0	260.0	45.826
C_0 = 50 mg/L, Q = 10 mL/min	3.0	3,450.0	345.0	50.188
	4.0	4,800	480	56.901

of the adsorbent. Whereas, at a lower flow rate, vanadium solution gets sufficient time to diffuse into the pores [23,24].

3.4. Effect of amino-pGMA bed height

The experiments were carried out at bed height, Z = 2, 3, and 4 cm while keeping the flowrate, and influent concentration constant. Fig. A2 elicits the effect of bed height on the dynamic adsorption of vanadium from solution. The breakthrough volume, time, and adsorption capacities are shown in Table 2. The results suggest that the column exhaustion time was slower on increasing the bed height from 2 to 4 cm. When the bed height is high, the diffusion of the vanadium toward solid-phase dominates the adsorption, and vanadium gets more time to diffuse towards this phase [22]. As a result, the treated volume (V_e) before column exhaustion also increased. The uptake capacity of the adsorbent increased on increasing the bed height due to the residential time increase of the solution inside the column bed. Thus, it can be concluded from these results that increasing bed height, decreasing the influent concentration, and flow rate influence the column adsorption capacity positively. However, as elicited in Table 2, the highest adsorption capacity of 75.5 mg/g was observed under Z = 3 cm, C_0 = 75 mg/L, and Q = 7.5 mL/min; thus, it is critical to optimize the bed operating parameters. The adsorption of vanadium on activated carbon modified with iron was 313 mg/g [25], while coal elicted an adsorption capacity of 60 mg/g [1]. Humic acid showed an adsorption capacity of 19.2 mg/g [26]; therefore, amino-pGMA has a competitive adsorption capacity of vanadium.

3.5. Dynamic bed optimization models

A proper design of a column adsorption process needs to have a prediction of the concentration, time profile, or breakthrough curve for outflow [9]. To study the fixed-bed column behavior Yoon–Nelson and Thomas were utilized to approximate breakthrough curves. The bed depth service time (BDST) model was also used to predict the breakthrough curves for different experiments at different conditions.

3.5.1. Thomas model

The experimental data obtained from dynamic column adsorption were analyzed to evaluate the kinetic uptake of vanadium by amino-pGMA. Experimental data were fitted by the Thomas model. The Thomas model assumes that the adsorption followed the Langmuir isotherm of adsorption-desorption, and axial dispersion does not occur in the column [17]. Using the equations illustrated in Table 1, the breakthrough curves were theoretically obtained and then paralleled against the experimentally attained breakthrough to establish the significance levels of the model. The Thomas rate constant (K_{TH}), uptake capacity (q_e), and coefficient correlation (R^2) were found by applying linear regression; results are summarized in Table 3. The $R^2 > 0.90$ at all tested conditions, thus, the correlation between C_t/C_0 and t in the Thomas model is high. As the initial vanadium concentration increased, the K_{TH} increased; therefore, the driving force during adsorption is concentration difference. Mass transfer is a common phenomenon often present in

Table 3
Thomas model parameters at different operating conditions using linear regression analysis

C_0 (mg/L)	Q (mL/min)	Z (cm)	$K_{TH} \times 10^2$- (mL/min/mg)	q_e (mg/g)	R^2
100	10.0	3.0	32.0	22.50	0.93
75	10.0	3.0	33.0	25.16	0.97
50	10.0	3.0	32.0	43.97	0.98
75	7.5	3.0	24.0	53.03	0.95
75	12.5	3.0	81.0	17.66	0.97
50	10.0	2.0	42.0	43.04	0.93
50	10.0	4.0	22.0	46.67	0.99

the adsorption process, and it influences the adsorption process, but Thomas model is only based on the reversible reaction kinetics. Therefore, the design of adsorption system based entirely on the Thomas model may be misleading. In addition, Yoon–Nelson model was also applied to analyze the breakthrough performance of a fixed-bed column.

An elementary theoretical model made by Yoon–Nelson was applied to observe the breakthrough behavior of vanadium on the amino-functionalized polymer. The Yoon–Nelson model assumes that the rate of decrease of adsorption probability for each adsorbate molecule is proportional to the probability of adsorbate adsorption and adsorbate breakthrough on the adsorbent [18]. K_{YN} and τ in the model represent rate constant and time required for 50% vanadium breakthrough, respectively.

3.5.2. Yoon–Nelson model

The experimental breakthrough vs. theoretically calculated breakthrough using Yoon–Nelson model equation fits better than the Thomas model. Using Yoon–Nelson model it was observed at higher flow rates and concentrations, the rate of adsorption increased and the time needed for 50% of the column to be exhausted, K_{YN} increased, and τ decreased. However, when the bed depth increased, τ increased while the values of K_{YN} lowered. The breakthrough curves at different operational conditions align almost perfectly with the experimentally attained data. The high coefficient of correlation further asserts the validity of the kinetic adsorption process described by this model, and the achieved results are experimentally justified. The calculated K_{YN} and τ are shown in Table 4.

3.5.3. BDST model

The performance of the practical scale column bed can be predicted by analyzing the data obtained from the laboratory-scale column bed. For this purpose, the BDST model has been widely used. The experimental data obtained at different flow rates were employed to BDST model to evaluate how the column design changes with different bed height. The BDST plots are shown in Fig. A3 and elicits linearity with the experimental data. The K_{OBDST} is the rate of vanadium transfer from the liquid phase to the solid phase of the column bed; K_{OBDST} decreased with increasing bed depth, as shown in Table 5. Therefore, short critical bed height is required for slow flow rate whereas, for high flow rate, the adsorption system requires longer critical BDST.

The bed capacity N_0 (mg/L) and rate constant K_{OBDST} (L/mg/min) from BDST model were obtained by plotting the service time t (min) vs. bed depth Z (cm) at C_i/C_0 as seen in Fig. A3. The service time experimental (t) and predicted service time (t_p) for the varying bed depth (2, 3, and 4 cm), flow rate, and influent concentration were calculated in Table 5. The values of the service time predicted by the BDST model are not a perfect fit but in good agreement

Table 4
Yoon–Nelson model parameters at different operational conditions

C_0 (mg/L)	Q (mL/min)	Z (cm)	K_{YN} (×10^{-5}) 1/min	τ (min)	R^2
100	10	3	32	45	0.94
75	10	3	25	67	0.98
50	10	3	16	175	0.99
75	7.5	3	17	200	0.96
75	12.5	3	61	38	0.98
50	10	2	24	118	0.99
50	10	4	12	270	0.99

Table 5
BDST model parameters at different operational conditions

Bed depth (cm)	Z = 4	Z = 3	Z = 2
K_{OBDST}	0.00026	0.000325	0.000478
N_0	10,733.30	9,275.52	9,476.38
R^2	0.9885	0.9958	0.9527
Flow rate (mL/min)	7.5	10.0	12.5
K_{OBDST}	0.000207	0.000344	0.000889
N_0	12,223.92	5,348.65	3,801.55
R^2	0.9866	0.9784	0.9786
C_0 (mg/L)	100	75	50
K_{OBDST}	0.00344	0.0003438	0.000325
N_0	5,025.79	5,348.65	9,277.60
R^2	0.9387	0.9784	0.988

with the experimental values of service time. Hence, this model could serve as a baseline in predicting critical bed depth required to remove vanadium with amino-pGMA.

4. Conclusion

The increased application of vanadium in both industries and the medical sector means increased exposure to humans and the environment. We investigated the removal of vanadium from water using amino-functionalized polymeric adsorbent resins in a fixed bed columns. The effects of bed height, feed flow rate, and initial concentration on the adsorption process were examined. The column was subjected to operate under various initial concentrations (C_0 = 100, 75, and 50 mg/L), bed depth (Z = 2, 3, and 4 cm), and feed flowrate (Q = 7.5, 10, and 12.5 mL/min). The highest adsorption capacity (q_e) of 75.5 mg/g was attained at C_0 = 75 mg/L, Z = 3 cm, and Q = 7.5 mL/min. The column was further optimized using Thomas, Yoon–Nelson, and bed-depth service time model equations to understand the breakthrough behavior and adsorption kinetics of amino-pGMA. The behaviors of the breakthrough curves were fitted best by Yoon–Nelson model at different conditions. The BDST model, as well as the Thomas model, elicited good comparison with the experimental data. FTIR showed a successful formation of amino-pGMA. The adsorption of vanadium was through NH_2–V–OH bond formation.

References

[1] G.W. Kajjumba, S. Aydın, S. Güneysu, Adsorption isotherms and kinetics of vanadium by shale and coal waste, Adsorpt. Sci. Technol., 36 (2018) 936–952.

[2] A. Evans, V. Strezov, T.J. Evans, Assessment of utility energy storage options for increased renewable energy penetration, Renewable Sustainable Energy Rev., 16 (2012) 4141–4147.

[3] G.W. Kajjumba, E. Yildirim, F. Osra, S. Aydin, T.T.K. Ngan, S. Emik, Insights into nonlinear adsorption kinetics and isotherms of vanadium using magnetised coal-polyaniline, Desal. Water Treat., 172 (2019) 158–166.

[4] N.K. Lazaridis, M. Jekel, A.I. Zouboulis, Removal of Cr(VI), Mo(VI), and V(V) ions from single metal aqueous solutions by sorption or nanofiltration, Sep. Sci. Technol., 38 (2003) 2201–2219.

[5] L.P.M. Lamers, How nitrate leaching from agricultural lands provokes phosphate eutrophication in groundwater fed wetlands: the sulphur bridge, Biogeochemistry, 98 (2010) 1–7.

[6] Y. Zhou, Q. Zhu, W. Ma, B. Xia, X. Xiao, Y. Zhao, P. Wang, H. Shi, Y. Zeng, Y. Zhang, Prenatal vanadium exposure, cytokine expression, and fetal growth: a gender-specific analysis in Shanghai MCPC study, Sci. Total Environ., 685 (2019) 1152–1159.

[7] G.W. Kajjumba, E. Yıldırım, S. Aydın, S. Emik, T. Ağun, F. Osra, J. Wasswa, A facile polymerisation of magnetic coal to enhanced phosphate removal from solution, J. Environ. Manage., 247 (2019) 356–362.

[8] H.M. Nur, B. Yüzer, M.İ. Aydin, S. Aydin, A. Öngen, H. Selçuk, Desalination and fate of nutrient transport in domestic wastewater using electrodialysis membrane process, Desal. Water Treat., 172 (2019) 323–329.

[9] C. Sarici-Ozdemir, M. Onay, Determination of parameters in fixed bed with industrial waste used as adsorbent, J. Phys. Chem. Funct. Mater., 1 (2018) 25–33.

[10] I. Zucker, H. Mamane, A. Riani, I. Gozlan, D. Avisar, Formation and degradation of N-oxide venlafaxine during ozonation and biological post-treatment, Sci. Total Environ., 619–620 (2018) 578–586.

[11] G.W. Kajjumba, S. Emik, A. Öngen, H. Kurtulus Özcan, S. Aydın, Modelling of Adsorption Kinetic Processes—Errors, Theory and Application, S. Edebali, Ed., Advanced Sorption Process Applications, IntechOpen, London, UK, 2018, pp. 1–9. Available at: https://www.intechopen.com/books/advanced-sorption-process-applications/modelling-of-adsorption-kinetic-processes-errors-theory-and-application

[12] Q. He, S. Si, J. Zhao, H. Yan, B. Sun, Q. Cai, Y. Yu, Removal of vanadium from vanadium-containing wastewater by amino modified municipal sludge derived ceramic, Saudi J. Biol. Sci., 25 (2018) 1664–1669.

[13] K.A. Bennani, B. Mounir, M. Hachkar, M. Bakasse, A. Yaacoubi, Adsorption of cationic dyes onto Moroccan clay: application for industrial wastewater treatment, J. Mater. Environ. Sci., 6 (2015) 2483–2500.

[14] H. Patel, Fixed - bed column adsorption study : a comprehensive review, Appl. Water Sci., 9 (2019) 1–17.

[15] S. Şahin, S. Emik, Fast and highly efficient removal of 2,4-D using amino-functionalized poly (glycidyl methacrylate) adsorbent: optimization, equilibrium, kinetic and thermodynamic studies, J. Mol. Liq., 260 (2018) 195–202.

[16] S. Emik, Preparation and characterization of an IPN type chelating resin containing amino and carboxyl groups for removal of Cu(II) from aqueous solutions, React. Funct. Polym., 75 (2014) 63–74.

[17] H.C. Thomas, Heterogeneous ion exchange in a flowing system, J. Am. Chem. Soc., 66 (1944) 1664–1666.

[18] Y.H. Yoon, J.H. Nelson, Application of gas adsorption kinetics — II. A theoretical model for respirator cartridge service life and its practical applications, Am. Ind. Hyg. Assoc. J., 45 (1984) 517–524.

[19] A.A. Ahmad, B.H. Hameed, Fixed-bed adsorption of reactive azo dye onto granular activated carbon prepared from waste, J. Hazard. Mater., 175 (2010) 298–303.

[20] E. Malkoc, Y. Nuhoglu, Y. Abali, Cr(VI) adsorption by waste acorn of Quercus ithaburensis in fixed beds: prediction of breakthrough curves, Chem. Eng. J., 119 (2006) 61–68.

[21] Y. Liu, Y. Li, Y. Hu, K.M.G. Mostofa, S. Li, Z. Liu, Y. Zhang, Adsorption characteristics and transport behavior of Cr(VI) in shallow aquifers surrounding a chromium ore processing residue (COPR) dumpsite, J. Chem., 2019 (2019) 1–10, doi: 10.1155/2019/4932837.

[22] D.K. Singh, V. Kumar, S. Mohan, D. Bano, S.H. Hasan, Breakthrough curve modeling of graphene oxide aerogel packed fixed bed column for the removal of Cr(VI) from water, J. Water Process Eng., 18 (2017) 150–158.

[23] J. López-Cervantes, D.I. Sánchez-Machado, R.G. Sánchez-Duarte, M.A. Correa-Murrieta, Study of a fixed-bed column in the adsorption of an azo dye from an aqueous medium using a chitosan–glutaraldehyde biosorbent, Adsorpt. Sci. Technol., 36 (2018) 215–232.

[24] J.T. Nwabanne, P.K. Igbokwe, Adsorption performance of packed bed column for the removal of lead(II) using oil palm fibre, Int. J. Appl. Sci. Technol., 2 (2012) 106–115.

[25] H. Sharififard, F. Pepe, P. Aprea, B. de Gennaro, Chemical modification of activated carbon surface with iron functional groups for efficient separation of vanadium: batch and column study, Res. Chem. Intermed., 43 (2017) 6553–6570.

[26] Y. Yu, M. Liu, J. Yang, Characteristics of vanadium adsorption on and desorption from humic acid, Chem. Ecol., 34 (2018) 548–564.

Appendix

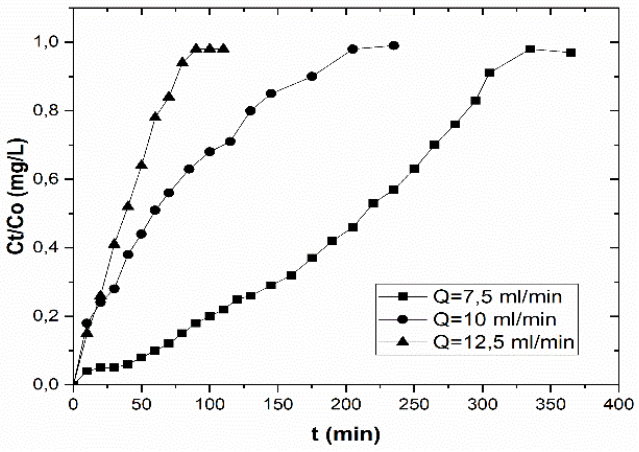

Fig. A1. Dynamic adsorption of vanadium on amino-pGMA at different flowrates (bed height = 3 cm, C_0 = 75 mL/min, pH = 4.5, and temperature = 22°C ± 1°C).

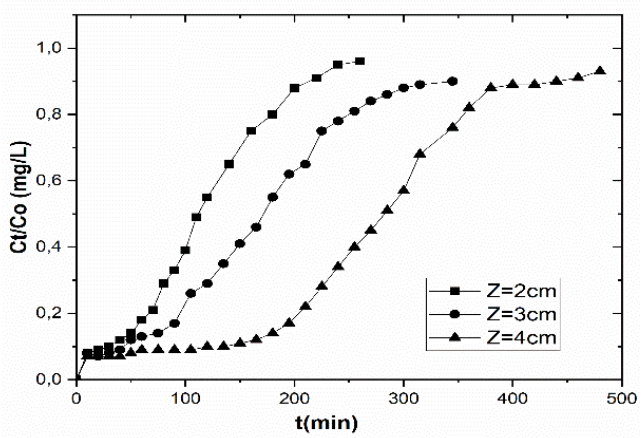

Fig. A2. Effect of bed height on the breakthrough curve.

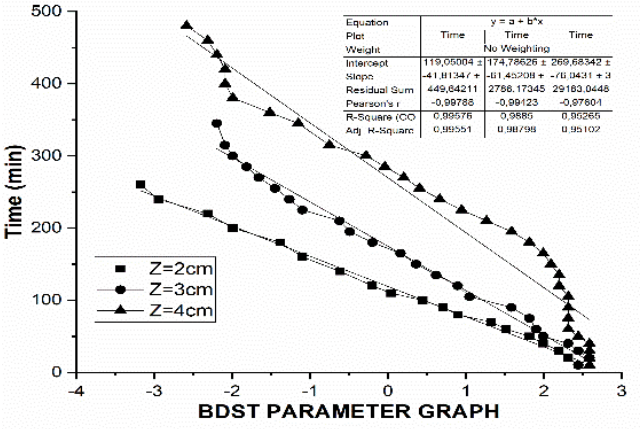

Fig. A3. BDST parameter graph at different bed height.